5350 *Biochemistry* **2009,** *48,* 5350–5357
DOI: 10.1021/bi900454s

BIOCHEMISTRY
including biophysical chemistry & molecular biology
Article

A Rotary Mechanism for Coenzyme B_{12} Synthesis by Adenosyltransferase[†]

Dominique Padovani and Ruma Banerjee*

Department of Biological Chemistry, University of Michigan Medical Center, Ann Arbor, Michigan 48109-5606

Received March 16, 2009; Revised Manuscript Received May 4, 2009

ABSTRACT: Adenosyltransferases (ATRs) catalyze the synthesis of the reactive cobalt−carbon bond found in coenzyme B_{12} or 5′-deoxyadenosylcobalamin (AdoCbl), which serves as a cofactor for a number of isomerases. The reaction involves a reductive adenosylation of cob(II)alamin in which an electron delivered by a reductase reduces cob(II)alamin to cob(I)alamin, which attacks the 5′-carbon of ATP to form AdoCbl and inorganic triphosphate. Of the three classes of ATRs found in nature, the PduO type, which is also the only one found in mammals, is the most extensively studied. The crystal structures of a number of PduO-type ATRs are available and reveal a trimeric organization with the active sites located at the subunit interfaces. We have previously demonstrated that the ATR from *Methylobacterium extorquens*, which supports methylmalonyl-CoA mutase activity, serves dual functions; i.e., it tailors the active AdoCbl form of the cofactor and then transfers it directly to the dependent mutase (Padovani et al. (2008) *Nat. Chem. Biol. 4*, 194). Only two of the three active sites in ATR are simultaneously occupied by AdoCbl. In this study, we demonstrate that binding of the substrate ATP to ATR that is fully loaded with AdoCbl leads to the ejection of 1 equivalent of the cofactor into solution. In the presence of methylmalonyl-CoA mutase and ATP, AdoCbl is transferred from ATR to the acceptor protein in a process that exhibits an ∼3.5-fold lower K_{act} for ATP compared to the one in which cofactor is released into solution. Furthermore, ATP favorably influences cofactor transfer in the forward direction by reducing the ratio of apo-methylmalonyl-CoA mutase/holo-ATR required for delivery of 1 equivalent of AdoCbl, from 4 to 1. These results lead us to propose a rotary mechanism for ATR function in which, at any given time, only two of its active sites are used for AdoCbl synthesis and where binding of ATP to the vacant site leads to the transfer of the high value AdoCbl product to the acceptor mutase.

Vitamin B_{12} or cobalamin is an organometallic cofactor that supports the activities of enzymes in organisms ranging from bacteria to man (*1*). Although the pathway for de novo synthesis of B_{12} shows limited prevalence in nature, the ability to tailor inactive cofactor transported into cells into the active forms exists in all B_{12}-utilizing organisms. In humans, the two active cofactor forms are methylcobalamin and 5′-deoxyadenosylcobalamin (AdoCbl[1] or coenzyme B_{12}) that support the activities of methionine synthase and methylmalonyl-CoA mutase (MCM), respectively. Tailoring of AdoCbl from inactive cobalamin precursors involves a reductive adenosylation step, which is catalyzed by adenosyltransferases (ATRs). Three varieties of ATRs belonging to the CobA, PudO, and EutT families exist and either support the de novo biosynthesis of AdoCbl (CobA) or are dedicated to specifically supporting propanediol or methylmalonyl-CoA metabolism (PduO) or to growth on ethanolamine (EutT) (*2*−*4*). Although members of all three ATR families catalyze the same overall reaction, they are not sequence relatives and therefore represent an evolutionary convergence on the same chemical solution, i.e., transfer of the adenosyl moiety of ATP to cob(I)alamin with concomitant elimination of inorganic triphosphate.

In organisms that have the capacity for de novo synthesis, AdoCbl represents the culmination of a pathway comprising over 2 dozen enzymes; i.e., it is a high-value product (*5*, *6*). Organisms like mammals that lack this pathway but utilize B_{12} to catalyze essential reactions have proteins that bind the cofactor avidly exhibiting submicromolar to femtomolar affinity (*7*). The relative rarity of the cofactor presents a challenge for cells for safeguarding against losses due to dilution. We have postulated that the PduO-type ATRs, which catalyze the ultimate step in AdoCbl assimilation and are needed by specific AdoCbl-dependent mutases, also serve as escorts for targeted delivery of the cofactor to dependent enzymes (*8*). Evidence for this hypothesis was recently furnished by kinetic studies combined with simulations, which demonstrated that AdoCbl is transferred directly between the active sites of recombinant *Methylobacterium extorquens* ATR and MCM from the same organism (*9*).

Bacterial and human ATRs that support MCM activity bind AdoCbl in the "base-off" state (*9*, *10*); i.e., the endogenous 5,6-dimethylbenzimidazole base is not coordinated to the cobalt atom in the corrin ring (Figure 1). A mirror "base-off" state of

[†]This work was supported in part by a grant from the National Institutes of Health (DK45776).

*Corresponding author. E-mail: rbanerje@umich.edu.

[1]Abbreviations: AdoCbl, 5′-deoxyadenosylcobalamin or coenzyme B_{12}; ATR, adenosyltransferase; mant-ATP, 2′(3′)-*O*-(*N*-methylanthraniloyl) adenosine 5′-triphosphate; MCM, methylmalonyl-CoA mutase.

 Published on Web 05/04/2009

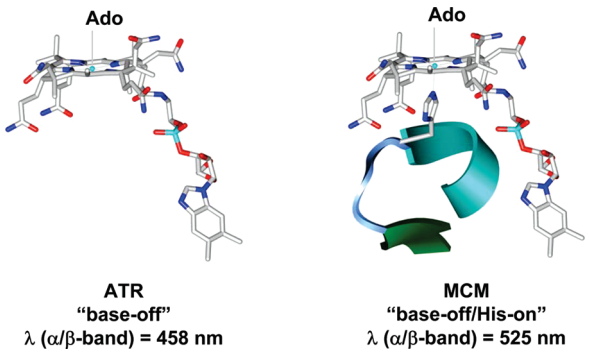

FIGURE 1: Schematic representation of the AdoCbl conformations in ATR and MCM as well as their principal absorption features.

AdoCbl bound to MCM is seen. However, a histidine residue donated by the mutases occupies the lower axial ligand position, giving rise to the so-called "base-off/His-on" state (*11*) (Figure 1). This difference in the coordination state leads to large changes in the absorption maxima of AdoCbl in the two active sites and provides a convenient means for tracking the cofactor. The direct transfer of AdoCbl from ATR to MCM is facilitated by the histidine residue on MCM that becomes the lower axial ligand as the cofactor moves from a 5- to a 6-coordinate environment (*9*). The strategy of mobilizing a cofactor from a low to a high coordination environment is deployed in the assembly of other metalloenzymes where the metal cofactor is conveyed from the donor to acceptor protein via sequential ligand-exchange reactions (*12*, *13*).

The structures of the human (*14*) and several bacterial (*15*−*17*) PduO-type ATRs have been reported. In all cases, the protein is a trimer, and the active sites are formed at the subunit interfaces. In the human enzyme, ATP was bound to two of the three active sites (*14*). This is consistent with functional data on the *M. extorquens* enzyme, which reveals nonequivalent active sites (*9*). Extensive kinetic and thermodynamic analyses on the *M. extorquens* ATR show that it displays negative cooperativity with only two of the active sites being simultaneously occupied by AdoCbl (*9*). The transfer kinetics for AdoCbl from ATR to MCM are biphasic, further confirming the existence of asymmetry. However, nonequivalent active sites are not apparent in the crystal structures of ATR from *Lactobacillus reuteri* in which three cob(II)alamin and/or three ATP molecules are bound per trimer (*16*, *17*). It is unclear whether this difference stems from the behavior of the protein in the solution versus the crystalline state or from the proteins being derived from different organisms. Given the high similarity in the sequences and in the structures of PduO-type ATRs that have been described so far (*14*−*17*), conservation of their ligand binding strategy and reaction mechanism might be expected.

Binding of ATP, which is presumed to be the first substrate to bind (*18*), occurs at the bottom of a cavernous pocket and results in the organization of an otherwise disordered N-terminal loop (*14*, *17*). Cob(II)alamin binds above ATP, sealing off the pocket. A C-terminal hinged lid clamps onto the cobalamin substrate and results in repositioning of a phenylalanine residue that plays a key role in enforcing the "base-off" conformation of the bound cofactor (*16*, *19*). The "base-off" conformation is advantageous for the reduction of cob(II)alamin and serves to increase its redox potential by ~100 mV (*20*). It is presently unclear whether a shared or a dedicated reductase in humans catalyzes the reduction of ATR-bound cob(II)alamin to generate the supernucleophilic cob(I)alamin species, which subsequently attacks the 5′-carbon of ATP to generate AdoCbl.

The direct transfer of AdoCbl from the *M. extorquens* ATR to MCM was found to be reversible and, in fact, favored cofactor transfer in the reverse direction, i.e., from MCM to ATR (*9*). Furthermore, the stoichiometry of the acceptor/donor proteins for the transfer of 1 equivalent of AdoCbl was four MCMs to one ATR (*9*). These observations raise several questions. How is the equilibrium for AdoCbl transfer from ATR to MCM shifted in favor of MCM in the cell? Is the transfer process triggered by a ligand-induced conformational change in the donor protein? Is the stoichiometry of the donor/acceptor protein pair modulated by binding of a ligand to ATR? To address these questions, we have examined the effect of binding of the substrate, ATP, on release of the product, AdoCbl, from ATR and demonstrate how it influences the transfer process. These studies lead us to formulate a rotary model for the operation of ATR in which the active sites are used sequentially to synthesize and then to transfer AdoCbl in a process that is coordinated by ATP binding.

EXPERIMENTAL PROCEDURES

Materials. AdoCbl and ATP were purchased from Sigma. The fluorescent analogue of ATP, 2′(3′)-*O*-(*N*-methylanthraniloyl)-ATP (mant-ATP) was purchased from Jena Biosciences (Germany).

Enzyme Expression and Purification. Recombinant *M. extorquens* MCM and ATR expressed in *Escherichia coli* were purified as previously described (*9*).

Isothermal Titration Calorimetry (ITC). The calorimetric titration experiments were performed in quadruplicate as described previously, and the data were analyzed using Microcal ORIGIN software (*9*). Briefly, the binding of ATP to ATR was monitored as follows. Enzyme (30−60 μM apo-ATR) in 50 mM Hepes buffer, pH 8.0, containing 0.3 M KCl, 10 mM $MgCl_2$, and 5% glycerol (buffer A) was titrated with 45 6.5 μL aliquots of a 0.75−1.5 mM solution of ATP at 20.0 ± 0.1 °C. The calorimetric signals were integrated, and the data were well fitted to a two-site binding model to estimate the equilibrium association constant, K_A, and the binding enthalpy, $\Delta H°$. The Gibbs free energy of binding, $\Delta G°$, and the entropic contribution to the binding free energy, $-T\Delta S°$, were calculated using eqs 1 and 2.

$$\Delta G° = -RT \ln K_A \quad (1)$$

$$\Delta G° = \Delta H° - T\Delta S° \quad (2)$$

UV−*Visible Spectroscopy*. *(i) Effect of ATP on Holo-ATR*. The effect of ATP binding to ATR fully reconstituted with 2 equivalents of AdoCbl (holo-ATR) was monitored at 20 °C by adding ATP (0.125−10 mM) to holo-ATR (20−100 μM bound-AdoCbl) in buffer A. The data were acquired just after mixing, and the concentration of AdoCbl released after each ATP addition was estimated from the increase in absorbance at 525 nm ($\Delta\varepsilon_{525nm}$ = 6.69 mM^{-1} cm^{-1}). ATP-dependent AdoCbl release into solution from holo-ATR was separately confirmed by collecting the filtrate obtained by centrifuging the reaction mixture using a Centricon YM30 concentrator (5000 rpm, 45 min, 4 °C). The volume of the starting sample was ~200−250 μL, and the volume of the flow-through was ~180−230 μL. Analysis of the filtrate by UV−visible spectroscopy confirmed the presence of AdoCbl. Under similar conditions but in the absence of ATP, holo-ATR releases 3.6 ± 1.5% (n = 10) cofactor into solution.

(ii) van't Hoff Analysis of ATP-Induced Cofactor Release. The same experiment as described above was performed at various temperatures (6−32 °C) to determine the standard enthalpic ($\Delta H°$) and entropic ($\Delta S°$) changes for ATP-induced AdoCbl release from holo-ATR. Following each addition of ATP (0.1−9.5 mM) to holo-ATR (20−30 μM), the solution was incubated at the desired temperature for 10 min to allow for temperature equilibration prior to recording of the UV−visible spectrum. The amount of AdoCbl released following each addition of ATP was estimated using a $\Delta\varepsilon_{525nm} = 6.69\ mM^{-1}\ cm^{-1}$ and plotted versus the concentration of ATP. A hyperbolic fit to the data yielded the apparent activation constant ($K_{act(ATP)}$) at each temperature. The temperature dependence of the apparent association constant ($1/K_{act(ATP)} = K_{A,act(ATP)}$) was analyzed according to the van't Hoff equation (eq 3) to determine the thermodynamic parameters associated with ATP-induced cofactor release.

$$\ln K_{A,act(ATP)} = -\frac{\Delta H°}{RT} + \frac{\Delta S°}{R} \quad (3)$$

(iii) Effect of ATP on Cofactor Transfer between ATR and MCM. The transfer of AdoCbl between the two enzyme active sites (in buffer A) was monitored by absorption spectroscopy at 20 °C. In the forward direction, 8−12 μM holo-ATR (16−24 μM bound AdoCbl) was added to a final concentration of 8−240 μM apo-MCM that was preincubated ± ATP (up to 8.3 mM). In the reverse direction, apo-ATR (4−145 μM final concentration) preincubated ± ATP (up to 9.9 mM) was added to 11−13 μM holo-MCM (containing the same concentration of bound AdoCbl). The absorption spectrum was acquired 5 min after mixing. The amount of AdoCbl transferred was estimated from the increase (forward) or decrease (reverse) in absorbance at 525 nm ($\Delta\varepsilon_{525nm} = 7.75\ mM^{-1}\ cm^{-1}$). Mixing 12 μM holo-ATR and 48 μM apo-MCM leads to 2.9 ± 1.0% ($n = 5$, ± SD) of AdoCbl being released into solution and the reconstitution of active holo-MCM as described previously (*9*). In the presence of ATP (0.14−8.3 mM), the proportion of cofactor detected in solution was approximately the same (5.0 ± 1.3%, $n = 5$).

Stopped-Flow Spectroscopy. Rapid reaction kinetics were studied aerobically in the dark using a Hi-Tech Scientific SF-61DX2 stopped-flow spectrophotometer. All solutions were filtered through a 0.2 μm syringe filter (Nalgene) and then transferred to the loading syringes and allowed to equilibrate for at least 15 min before initiating the experiments. An external water bath was used to maintain the loading syringes and the mixing chamber at the desired temperature.

(i) Kinetic Analysis of Mant-ATP Binding to Apo-ATR. The experiments were performed at 20 °C in buffer A with a final concentration of ~1 μM mant-ATP and increasing concentrations of apo-ATR (5−30 μM). Mant-ATP was excited at 355 nm, and the emission was recorded using a 408 nm cutoff filter. The observed fluorescence transients were fitted to a double exponential function to obtain the pseudo-first-order rate constants, k_{obs1} and k_{obs2}, for ATP binding to sites 1 and 2, respectively, in ATR. The rate constants showed a linear dependence on protein concentration. The dissociation rate constants were obtained by mixing a preformed complex of mant-ATP−ATR (~1:50 μM) with 5 mM unlabeled ATP and by fitting the kinetic traces to a double exponential function to obtain the dissociation rate constants, k_{off1} and k_{off2} for mant-ATP release from the two binding sites of ATR. The kinetic simulation program, Berkeley Madonna 8.0.1 (www.berkeleymadonna.com), was used to fit the mant-ATP binding data according to a model describing successive binding of mant-ATP to the two binding sites in ATR (eq 4).

$$\mathrm{ATR} + \mathrm{ATP} \underset{k_{off1}}{\overset{k_{on1}}{\leftrightarrow}} (\mathrm{ATR{-}ATP}) + \mathrm{ATP} \underset{k_{off2}}{\overset{k_{on2}}{\leftrightarrow}} \mathrm{ATR(ATP)_2} \quad (4)$$

The curve fitting was performed using the Runge−Kutta 4 method. To simulate the mant-ATP binding data, the kinetic traces obtained at six protein concentrations were employed, and the experimentally determined dissociation rate constants (k_{off}) were constrained (within the SD range) and the association rate constants (k_{on1} and k_{on2}) were allowed to float.

(ii) Kinetic Analysis of AdoCbl Binding to Apo-ATR. Binding of AdoCbl to ATR was carried out in buffer A at 20 °C by rapidly mixing varying concentrations of AdoCbl (40−120 μM before mixing) with a fixed concentration of ATR (8−20 μM before mixing) and monitoring the decrease in A_{525nm} ($\Delta\varepsilon_{525nm} = -6.69\ mM^{-1}\ cm^{-1}$). The kinetic traces were best fit to a double exponential function to obtain k_{obs1} and k_{obs2} and the amplitude change associated with each phase, ΔA_1 and ΔA_2. The Berkeley Madonna 8.0.1 simulation program was used to fit the AdoCbl binding data according to eqs 5 and 6, which describe a model for AdoCbl binding to ATR as reported previously (*9*). Curve fitting was performed using the Runge−Kutta 4 method. To simulate the data, the kinetic traces obtained at five cofactor concentrations were employed.

$$\mathrm{ATR} + \mathrm{B_{12}} \underset{k_{off1}}{\overset{k_{on1}}{\leftrightarrow}} (\mathrm{ATR{-}B_{12}}) \underset{k_{conf-1}}{\overset{k_{conf1}}{\leftrightarrow}} (\mathrm{ATR{-}B_{12}})* \quad (5)$$

$$(\mathrm{ATR{-}B_{12}})* + \mathrm{B_{12}} \underset{k_{off2}}{\overset{k_{on2}}{\leftrightarrow}} [(\mathrm{ATR{-}B_{12}})* {-} \mathrm{B_{12}}] \underset{k_{conf-2}}{\overset{k_{conf2}}{\leftrightarrow}} (\mathrm{ATR{-}(B_{12})_2})* \quad (6)$$

The values for K_{D1} and K_{D2} were obtained using eq 7.

$$K_{D1} = \frac{\left(\frac{k_{off1}}{k_{on1}}\right)\left(\frac{k_{conf-1}}{k_{conf1}}\right)}{1 + \frac{k_{conf-1}}{k_{conf1}}} \quad \text{and} \quad K_{D2} = \frac{\left(\frac{k_{off2}}{k_{on2}}\right)\left(\frac{k_{conf-2}}{k_{conf2}}\right)}{1 + \frac{k_{conf-2}}{k_{conf2}}} \quad (7)$$

(iii) Kinetic Analysis of ATP-Induced AdoCbl Release from Holo-ATR. Release of cofactor from holo-ATR induced by ATP binding was investigated by rapidly mixing a fixed concentration of holo-ATR (20−40 μM before mixing) with increasing concentrations of ATP (0.1−20 mM before mixing) in buffer A at 20 °C. Cofactor release was monitored at 525 nm. Kinetic traces were best fitted to a double exponential function to obtain the pseudo-first-order rate constants for AdoCbl release (k_{obs1} and k_{obs2}) and the change in amplitude (ΔA_1 and ΔA_2) associated with each phase. The data were analyzed by plotting both k_{obs1} and k_{obs2} as a function of ATP concentration and fitted to a hyperbolic decay function, yielding the values for k_{obs1} and k_{obs2} when [ATP] → 0 and [ATP] → ∞.

RESULTS AND DISCUSSION

Structural studies on PduO-type ATRs have revealed that these trimeric proteins contain active sites at the subunit interfaces (*14*−*17*), while spectroscopic studies reveal that they utilize only two of the three active sites at a time (*9*). The trimer binds 2 mol of AdoCbl in an atypical "base-off" conformation in which the endogenous ligand, 5,6-dimethylbenzimidazole, is not coordinated to the cobalt atom (*9*, *10*, *21*). In contrast, the

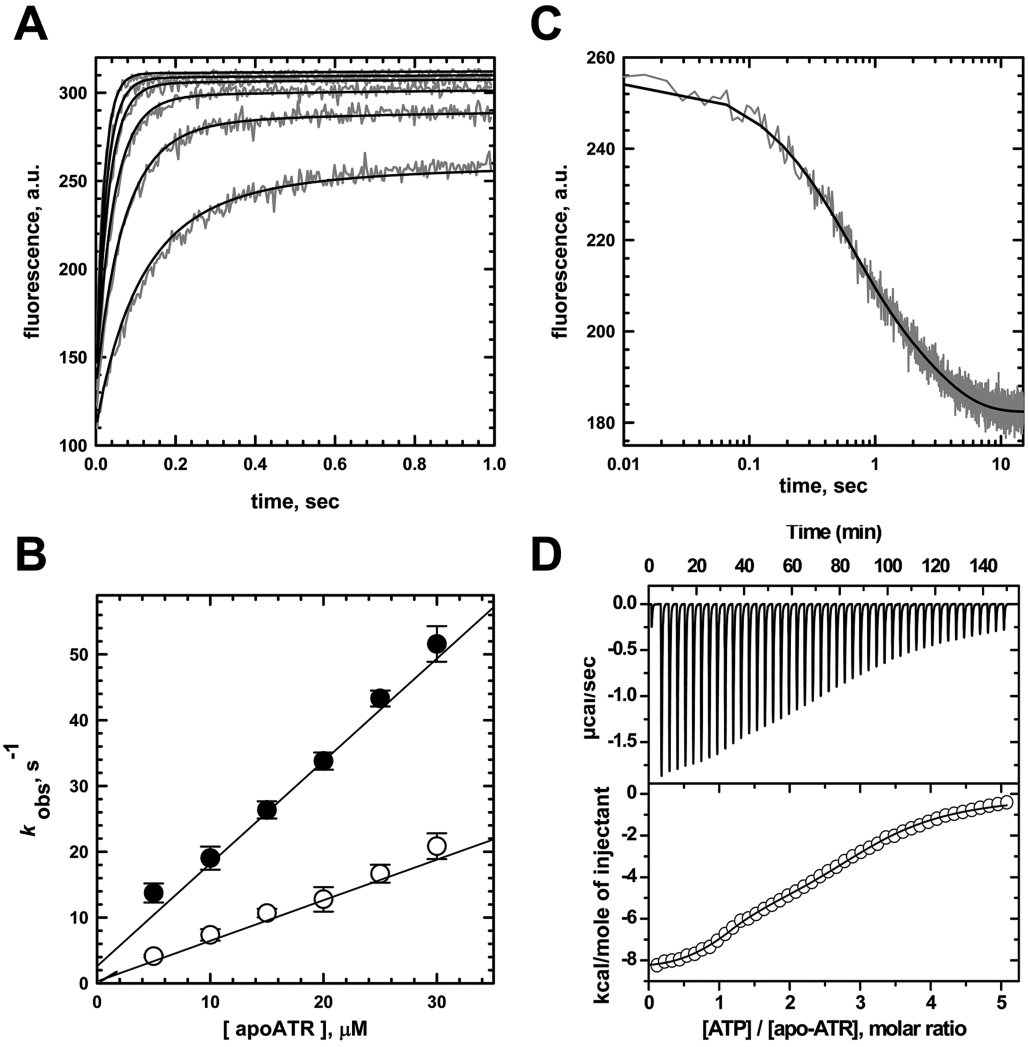

FIGURE 2: Binding of ATP to ATR. (A) Representative fluorescent transients observed by mixing 1 μM mant-ATP to increasing concentrations (5−30 μM) of ATR (gray lines) in buffer A at 20 °C. The simulations (black lines) were performed as described under Experimental Procedures and yielded the kinetic parameters reported in Table 1. (B) Dependence of the pseudo-first-order rate constants (k_{obs1}, ●, and k_{obs2}, ○) for mant-ATP binding on apo-ATR. The black lines represent the simulated fits to the experimental data. (C) Dissociation of mant-ATP (1 μM) from ATR (50 μM) was monitored in a displacement assay using 5 mM ATP (gray line). The kinetic trace was best fit to a double exponential function (black line) with $k_{obs1} = 1.84 \pm 0.16\ s^{-1}$ and $k_{obs2} = 0.3 \pm 0.02\ s^{-1}$ (three independent experiments). (D) Representative calorimetric titration data for binding of ATP to apo-ATR (40 μM) in buffer A at 20 °C. The top panel shows the raw data in power versus time. The area under each spike is proportional to the heat produced with each injection. The lower panel shows the integrated areas normalized to the number of moles of ATP added with each injection. The data were well fit to a two-site binding model and yielded the thermodynamic parameters for ATP binding reported in the Table 2.

AdoCbl acceptor protein, MCM, binds its cofactor in the "base-off/His-on" state in which the lower axial ligand is displaced by a histidine residue donated by the active site (*11*, *22*). These coordination state differences result in large changes in the absorption spectra of AdoCbl bound to the two proteins (Figure 1) and facilitated earlier investigations on the mechanism of cofactor transfer between the two active sites (*9*). Surprisingly, the transfer of AdoCbl between ATR and MCM, in the absence of other ligands or proteins, was found to be readily reversible and, in fact, favored the reverse direction, i.e., from MCM to ATR (*9*). In comparison to the low (micromolar) K_M for ATP binding to ATR, the intracellular concentration of ATP is high (in the millimolar range), conditions that would favor ATP binding to ATR. In this study, we have examined how binding of ATP to ATR influences dislocation of the product, AdoCbl, influences the stoichiometry of the protein−protein interaction needed for cofactor transfer, and thereby modulates the equilibrium for AdoCbl transfer between the two proteins.

Stoichiometry of ATP Binding to ATR. The binding of ATP to ATR was characterized by stopped-flow fluorescence spectroscopy and by isothermal titration calorimetry (Figure 2). The kinetics of ATP binding to apo-ATR were analyzed using the fluorescent ATP derivative, mant-ATP. Fluorescent analogues of nucleotides have been widely used to study nucleotide binding by proteins as they are environmentally responsive and sensitive probes for detecting conformational changes, e.g., in protein−nucleotide complexes (*23*, *24*). The fluorescence of mant-ATP increases upon binding to apo-ATR without any significant shift in the emission maximum (444 nm) (data not shown). The fluorescence transients, obtained under pseudo-first-order conditions, could be fit by a double exponential function (Figure 2A), yielding the pseudo-first-order rate constants k_{obs1} and k_{obs2}, which show a linear dependence on apo-ATR concentration (Figure 2B), consistent with the binding of two molecules of mant-ATP per trimer. Similarly, the observed rate constants for dissociation of mant-ATP from ATR, measured in

Table 1: Kinetic Parameters for Binding of Mant-ATP or AdoCbl to ATR[a]

	mant-ATP		AdoCbl[b]	
	site 1	site 2	site 1	site 2
k_{on}, μM^{-1} s^{-1}	1.63	0.3	6.54	7.9
k_{off}, s^{-1}	0.31	1.77	1176	1067
K_D, μM	0.19 ± 0.02	5.9 ± 1.4	0.14 ± 0.02	2.1 ± 0.5

[a] The kinetic parameters were obtained from simulations as described under Experimental Procedures. The values represent the mean of at least two independent simulations. The SD for each value was less than 15%. [b] The kinetic parameters for AdoCbl binding were obtained using eqs 5 and 6 as described under Experimental Procedures. The values obtained from the simulations for k_{conf1} and k_{conf-1} were 379 and 0.29 s^{-1}, respectively, and for k_{conf2} and k_{conf-2} were 72 and 1.2 s^{-1}, respectively.

a displacement assay, exhibit biphasic kinetics yielding values of 1.84 ± 0.16 and 0.3 ± 0.02 s^{-1} for the two phases (Figure 2C). The values of the two association rate constants (k_{on}) were obtained by global fitting of the fluorescence transients as described under Experimental Procedures and are reported in Table 1. An excellent correspondence was observed between the simulated and experimental data (Figure 2A,B), supporting the validity of the model with two mant-ATPs binding per trimer of ATR. The kinetically determined K_D values for binding of the fluorescent analogue to sites 1 and 2 are 0.19 ± 0.02 and 5.9 ± 1.4 μM. The values obtained for binding of ATP from calorimetric titration experiments are 0.6 ± 0.1 and 12.6 ± 2 μM, respectively (Table 2), and are in the range of the K_M values reported for other PduO-type ATRs (*2*, *17*, *25*). Based on the ITC data, binding of ATP to sites 1 and 2 is enthalpically driven.

Stoichiometry of AdoCbl Binding to ATR. We have previously characterized the K_Ds for AdoCbl binding to ATR (*9*). However, these studies were performed in 50 mM potassium phosphate buffer, pH 7.5, in contrast to buffer A used in this study. The switch in buffers was made since buffer A is compatible for studies involving all three proteins, ATR, the small G-protein chaperone, MeaB (*26*−*28*), and MCM involved in assimilation, docking, and usage, respectively, of AdoCbl. We have therefore redetermined the kinetic parameters for AdoCbl binding to ATR (Table 1). The kinetically determined K_D values for AdoCbl binding to ATR are 0.14 ± 0.02 and 2.1 ± 0.5 μM, respectively, and are similar to the values obtained previously in phosphate buffer (K_{D1} = 0.6 ± 0.1 μM and K_{D2} = 1.5 ± 0.4 μM) (*9*).

ATP Induces Release of 1 Equivalent of AdoCbl from ATR. When ATR reconstituted with 2 equivalents of AdoCbl is mixed with increasing concentrations of ATP, a partial conversion of the cofactor from the "base-off" to the "base-on" conformation is observed as evidenced by the increase in absorption at 525 nm and the decrease at 458 nm (Figure 3A). This spectral change occurs with isosbestic points at 337, 389, and 482 nm. The "base-on" species represents cofactor that is released into solution and can be recovered in the filtrate following centrifugation in a Centricon concentrator. At saturating ATP concentration, 50.5 ± 7.6% (1.0 ± 0.15 molecules) of AdoCbl initially bound to ATR is released (Figure 3 inset). The extent of cofactor released from holo-ATR after ATP addition (calculated with a $\Delta\varepsilon_{525nm} \sim 6.79$ mM^{-1} cm^{-1}) correlated well within experimental error to the concentration recovered in the filtrate. In contrast, in the absence of ATP, 3.6 ± 1.5% (n = 10) release of AdoCbl from ATR was observed. The van't Hoff analysis of the temperature dependence of $K_{act(ATP)}$ for ATP-induced release of

Table 2: Thermodynamic Parameters for Binding of ATP to ATR[a]

	ΔH, kcal/mol	$T\Delta S$, kcal/mol	ΔG, kcal/mol	K_D, μM
site 1	−8.1 ± 0.4	0.3 ± 0.3	−8.3 ± 0.1	0.60 ± 0.11
site 2	−6.0 ± 0.4	0.6 ± 0.5	−6.6 ± 0.4	12.6 ± 2.0

[a] Determined by ITC at 20 °C as described under Experimental Procedures. The values represent the mean of four independent experiments (±SD).

AdoCbl (Figure 3B) revealed that the overall process is thermodynamically favored, with $\Delta G° = -8.3 \pm 0.8$ kcal/mol at 20 °C (corresponding to a $K_{eq,app} = 1.45 \times 10^6$), and yielded values for $\Delta H°$ and $\Delta S°$ of −6.2 ± 0.4 kcal/mol and +7.1 ± 1.4 cal/(mol·K), respectively.

The kinetics of ATP-triggered AdoCbl release were monitored by stopped-flow spectrometry and were clearly biphasic, consistent with the release of the cofactor from both active sites. However, the amplitudes associated with the two phases are markedly different with $\Delta A_2 \sim 10\Delta A_1$ (Figure 3C), indicating that AdoCbl release occurs preferentially from one site. In contrast, in the absence of ATP, ~5% of the cofactor is released into solution, and the relative change in amplitude associated with the two phases is $\Delta A_1 \sim 3\Delta A_2$ (not shown). The observed rate constants for AdoCbl release exhibit a hyperbolic dependence on ATP concentration (Figure 3D), yielding values for $k_{obs1([ATP]\to\infty)}$ and $k_{obs2([ATP]\to\infty)}$ of 4.1 ± 2.0 and 0.19 ± 0.03 s^{-1}, respectively. When ATP concentration tends to zero, the values for $k_{obs1([ATP]\to0)}$ and $k_{obs2([ATP]\to0)}$ are 25.2 ± 8.1 and 0.72 ± 0.07 s^{-1}, respectively. The hyperbolic dependence of the pseudo-first-order rate constants can be explained by a model in which an isomerization step precedes B_{12} release as described below. Hence, ATP binds only to a "binding-ready" conformation of the holo-ATR complex, $[ATR\cdot(B_{12})_2]^*$.

$$[ATR\cdot(B_{12})_2] \underset{k_2}{\overset{k_1}{\leftrightarrow}} [ATR\cdot(B_{12})_2]^* \underset{k_4,\ -ATP}{\overset{k_3,\ ATP}{\leftrightarrow}} [ATR\cdot(B_{12}\cdot ATP)] + B_{12}$$

The isomerization rate constant, k_1, is slow, and in the absence of ATP, the isomerization equilibrium (k_2/k_1) favors the $[ATR\cdot(B_{12})_2]$ state, and B_{12} release only occurs from the small fraction of the enzyme in the $[ATR\cdot(B_{12})_2]^*$ state. In the presence of ATP, the equilibrium is drawn toward the right, and B_{12} release is limited by the slow isomerization step. For simplicity, the ATP binding and B_{12} release steps have been combined in the model described above. The observed rate constant k_{obs} is a complex function as described in eq 8, where $k_{obs([ATP]\to\infty)} = k_1$ and $k_{obs([ATP]\to0)} = k_4$.

$$k_{obs} = \frac{k_1[ATP] + \left(\frac{k_1+k_2}{k_3}\right)k_4}{[ATP] + \frac{k_1+k_2}{k_3}} \quad (8)$$

In stopped-flow fluorescence experiments performed with mant-ATP instead of ATP, the k_{obs} values showed the same hyperbolic decay dependence on mant-ATP concentration (data not shown). Furthermore, we have previously observed similar kinetic behavior for AdoCbl transfer from holo-ATR triggered by increasing concentrations of the acceptor, apo-MCM (*9*).

ATP Modulates AdoCbl Transfer between ATR and MCM. As reported previously (*9*), we found that in the absence of ATP the transfer of one AdoCbl from ATR to MCM in buffer A requires an acceptor/donor ratio of ~4 and, in fact, favors the

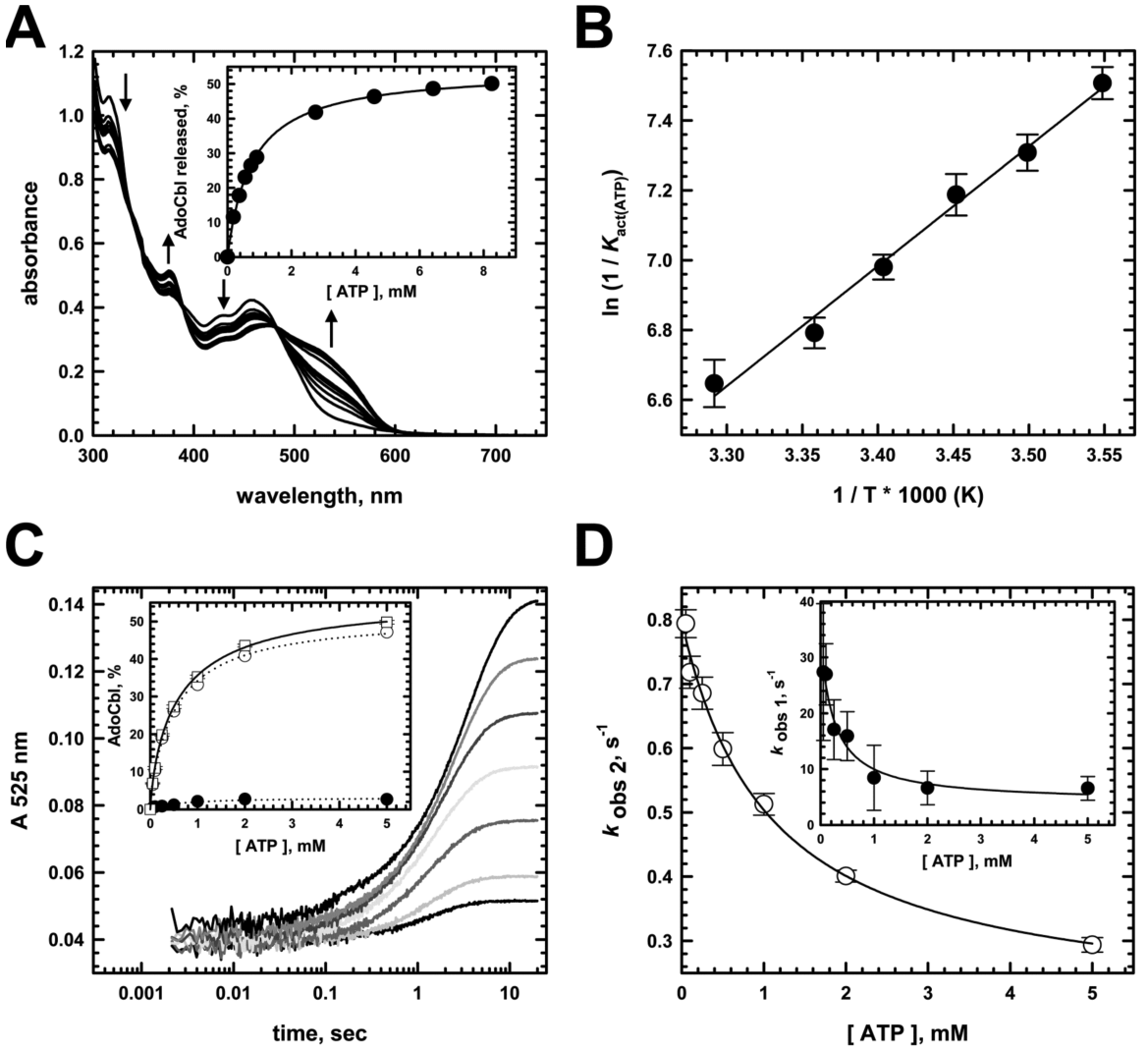

FIGURE 3: ATP induces release of one AdoCbl from holo-ATR. (A) Addition of ATP (0.2−8.2 mM) to holo-ATR (26.4 μM in bound AdoCbl) in buffer A at 20 °C results in the partial conversion of AdoCbl from the "base-off" to the "base-on" state. Inset: The ATP dependence of AdoCbl release reveals that only one of two molecules of cofactor bound per trimer is released to solution. (B) Analysis of the temperature dependence of the $K_{act(ATP)}$ for AdoCbl release by the van't Hoff equation yields the following values: $\Delta H° = -6.2 \pm 0.4$ kcal/mol, $\Delta S° = 7.1 \pm 1.4$ cal/(mol·K), and $\Delta G° = -8.3 \pm 0.8$ kcal/mol at 20 °C. (C) Data from a representative stopped-flow experiment for AdoCbl release from holo-ATR (31.3 μM in AdoCbl after mixing) in the presence of varying concentrations of ATP (0.05−5 mM after mixing, bottom to top) in buffer A at 20 °C. Inset: The ATP dependence of AdoCbl release from ATR (□) as determined from the stopped-flow spectrometry data confirms that only one of two molecules of cofactor is released into solution, with ○ and ● representing the contributions of the two sites to cofactor release. (D) Dependence of the pseudo-first-order rate constant for AdoCbl release, k_{obs2}, on ATP concentration. A hyperbolic fit to the data yields $k_{obs2[ATP]\to 0} = 0.72 \pm 0.07$ s^{-1} and $k_{obs2[ATP]\to\infty} = 0.19 \pm 0.03$ s^{-1} ($n = 3$). Inset: Dependence of the pseudo-first-order rate constant for AdoCbl release, k_{obs1}, on ATP concentration. A hyperbolic fit to the data yields $k_{obs1[ATP]\to 0} = 25 \pm 8$ s^{-1} and $k_{obs1[ATP]\to\infty} = 4.1 \pm 2.0$ s^{-1}.

reverse transfer, i.e., from MCM to ATR (Table 3) (*9*). Under these conditions, only 2.9 ± 1.0% ($n = 10$) of the cofactor was detected in solution, consistent with a direct transfer mechanism as described previously (*9*). Furthermore, MCM activity is dependent on ATR concentration, revealing that MCM is productively loaded with AdoCbl delivered by ATR (*9*). We have examined the effect of ATP on the acceptor/donor molar ratio at which the transfer of 1 equivalent of AdoCbl occurs. In the presence of ATP, 1 equivalent of AdoCbl is transferred when holo-ATR and apo-MCM are present at a molar ratio of 1 (Figure 4 and Table 3). The spectral changes accompanying cofactor transfer exhibit isosbestic points at 338, 392, and 487 nm, which are similar to the values reported previously for cofactor transfer between ATR and MCM (*9*) and slightly different from the one observed for ATP-induced release of AdoCbl into solution described above. The presence of ATP does not influence the activity of MCM as determined under steady-state conditions (data not shown). Significantly, the $K_{act(ATP)}$ for ATP in the AdoCbl transfer/release assay decreases from 869 ± 124 μM in the absence of MCM to 251 ± 11 μM in its presence, indicating that the ATP-driven AdoCbl expulsion from ATR occurs more efficiently when apo-MCM is present in the reaction mixture (Figure 4A

Table 3: ATP Influences AdoCbl Transfer between ATR and MCM[a]

	donor	
	holo-ATR	holo-MCM
([acceptor]/[donor])$_{[ATP]=0}$	4.0 ± 0.3	1.6 ± 0.2
([acceptor]/[donor])$_{[ATP]\to\infty}$	1.1 ± 0.1	29.7 ± 2.5

[a] The values represent the molar [acceptor]/[donor] ratio required to transfer 1 equivalent of AdoCbl.

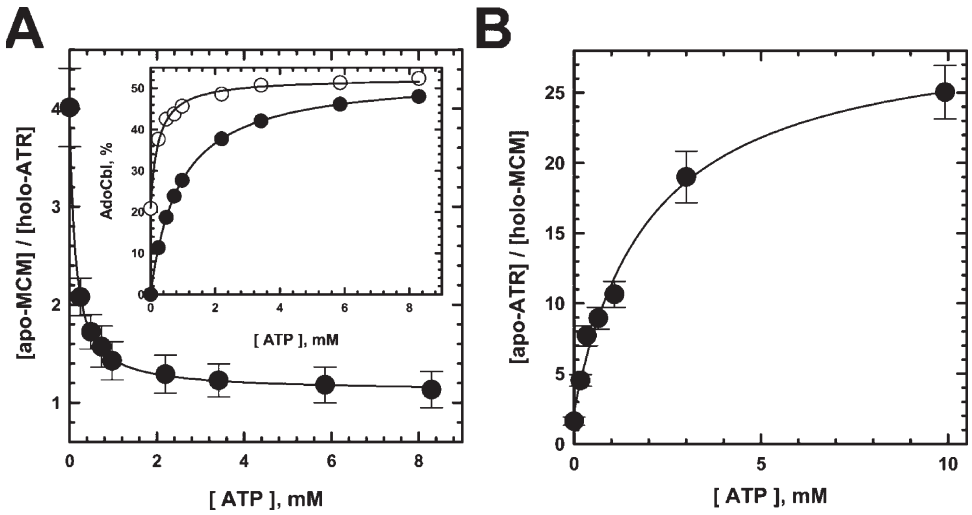

FIGURE 4: ATP influences the acceptor/donor molar ratio for AdoCbl transfer. (A) Dependence of the molar ratio of [apo-MCM]/[holo-ATR] on ATP concentration (0−8.3 mM) needed for the transfer of one AdoCbl. Inset: Effect of increasing ATP concentration (0−8.3 mM) on AdoCbl release from holo-ATR in the presence (○) or absence (●) of 1 equivalent of apo-MCM. Hyperbolic fits to the data yield values for $K_{act(ATP)}$ = 869 ± 124 μM (n > 10) and 251 ± 11 μM (n = 2) in the absence and presence of apo-MCM, respectively. (B) Dependence of the molar ratio, [apo-ATR]/[holo-MCM], on ATP concentration (0−9.8 mM) for transfer of 1 equivalent of AdoCbl.

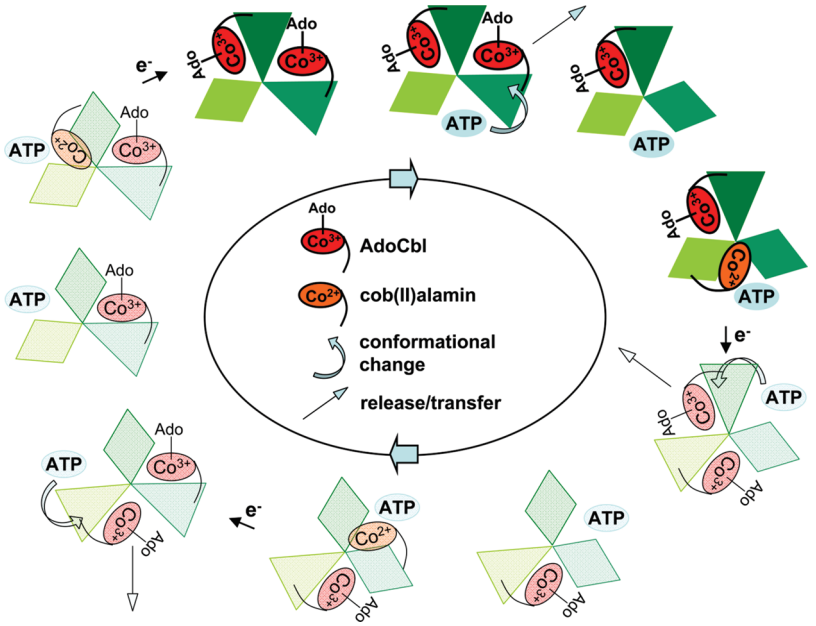

FIGURE 5: Model describing a rotary mechanism for AdoCbl synthesis and transfer from ATR.

inset). ATP negatively influences AdoCbl transfer in the reverse direction, i.e., from MCM to ATR. Thus, the molar ratio of [apo-ATR]/[holo-MCM] needed to transfer one molecule of cofactor from holo-MCM to apo-ATR increases from ~1.6 to ~29.7 in the absence and presence of ATP, respectively (Figure 4B and Table 3). The overall effect of ATP binding to ATR is to make AdoCbl transfer to MCM more favorable in the transient complex that forms between these two proteins.

A Rotary Mechanism for ATR Function. The architectural organization of ATR with three active sites at the subunit interfaces contrasts with its apparent usage of only two active sites at a time. Hence both kinetic and thermodynamic analyses of ATP and cobalamin binding reveal that only two of the three sites are occupied at any given time (Figure 2, Tables 1 and 2). In this study, we demonstrate that binding of ATP leads to jettisoning of one of the two AdoCbl molecules bound to ATR and suggests a sequential "rotary" mechanism for coenzyme B_{12} synthesis and delivery (Figure 5). In this model, ATP binding to sites 1 and 2 in ATR drives catalytic conversion of cobalamin to AdoCbl while binding to site 3 drives cofactor transfer, thereby emptying one of the active sites on ATR in preparation for another round of catalysis. A well-characterized example of an enzyme that uses a different rotary mechanism is ATP synthase in which the γ subunit of the ATP synthase complex rotates either clockwise or counterclockwise in ATP synthesis or ATP hydrolysis, respectively (*29*). In contrast, the rotary mechanism of ATR is predicted to follow a unidirectional track driven by ATP binding. Thus, a third of the cycle can be described as follows (Figure 5). ATP binding to site 3 in AdoCbl-loaded ATR leads to emptying of AdoCbl from site 1. On the basis of the structures of PduO-type ATRs, we speculate that rearrangement of the N-terminal domain triggered by binding of ATP (*14*, *17*) provokes a

conformational change in the adjacent subunit leading to cofactor transfer. Since MCM lowers the K_{act} for ATP by ~3.5-fold, its interaction with ATR apparently influences the conformational change induced by ATP. Deletion of six residues from the C-terminus of the *L. reuterii* PduO-type ATR leads to inactive AdoCbl biosynthesis *in vivo*, suggesting the involvement of this region in protein−protein interaction with MCM (*16*, *19*). Alternatively, holo-ATR might exist in a mixture of states with the N-terminal loop being either organized or disordered. Binding of ATP shifts the equilibrium to the N-terminal ordered conformation and promotes release/transfer of AdoCbl. Binding of cob(II)alamin to the ATP-containing subunit would then lead to another cycle of AdoCbl synthesis in the presence of a reductase. Thus, the dual function of ATR as the enzyme that catalyzes the ultimate step in AdoCbl assimilation and as an escort for targeted delivery of its product to MCM is tuned by binding of its substrate, ATP, which drives the synthesis/transfer steps in the forward direction.

REFERENCES

1. Banerjee, R., and Ragsdale, S. W. (2003) The many faces of vitamin B_{12}: Catalysis by cobalamin-dependent enzymes. *Annu. Rev. Biochem. 72*, 209–247.
2. Johnson, C. L., Buszko, M. L., and Bobik, T. A. (2004) Purification and initial characterization of the *Salmonella enterica* PduO ATP:cob(I)alamin adenosyltransferase. *J. Bacteriol. 186*, 7881–7887.
3. Buan, N. R., Suh, S. J., and Escalante-Semerena, J. C. (2004) The eutT gene of *Salmonella enterica* encodes an oxygen-labile, metal-containing ATP:corrinoid adenosyltransferase enzyme. *J. Bacteriol. 186*, 5708–5714.
4. Suh, S., and Escalante-Semerena, J. C. (1995) Purification and initial characterization of the ATP:corrinoid adenosyltransferase encoded by the cobA gene of *Salmonella typhimurium*. *J. Bacteriol. 177*, 921–925.
5. Battersby, A. (1994) How nature builds the pigments of life: The conquest of vitamin B_{12}. *Science. 264*, 1551–1557.
6. Scott, A. I. (1994) The discovery of nature's pathwaty to vitamin B_{12}. A 25 year odyssey. *Tetrahedron. 50*, 13315–13333.
7. Banerjee, R. (2006) B12 trafficking in mammals: A for coenzyme escort service. *ACS Chem. Biol. 1*, 149–159.
8. Yamanishi, M., Vlasie, M., and Banerjee, R. (2005) Adenosyltransferase: An enzyme and an escort for coenzyme B_{12}?. *Trends Biochem. Sci. 30*, 304–308.
9. Padovani, D., Labunska, T., Palfey, B. A., Ballou, D. P., and Banerjee, R. (2008) Adenosyltransferase tailors and delivers coenzyme B12. *Nat. Chem. Biol. 4*, 194–196.
10. Yamanishi, M., Labunska, T., and Banerjee, R. (2005) Mirror "base-off" conformation of coenzyme B_{12} in human adenosyltransferase and its downstream target, methylmalonyl-CoA mutase. *J. Am. Chem. Soc. 127*, 526–527.
11. Padmakumar, R., Taoka, S., Padmakumar, R., and Banerjee, R. (1995) Coenzyme B_{12} is coordinated by histidine and not dimethylbenzimidazole on methylmalnyl-CoA mutase. *J. Am. Chem. Soc. 117*, 7033–7034.
12. Pufahl, R. A., Singer, C. P., Peariso, K. L., Lin, S. J., Schmidt, P. J., Fahrni, C. J., Culotta, V. C., Penner-Hahn, J. E., and O'Halloran, T. V. (1997) Metal ion chaperone function of the soluble Cu(I) receptor Atx1. *Science. 278*, 853–856.
13. Tong, W. H., Jameson, G. N., Huynh, B. H., and Rouault, T. A. (2003) Subcellular compartmentalization of human Nfu, an iron-sulfur cluster scaffold protein, and its ability to assemble a [4Fe-4S] cluster. *Proc. Natl. Acad. Sci. U.S.A. 100*, 9762–9767.
14. Schubert, H. L., and Hill, C. P. (2006) Structure of ATP-bound human ATP:cobalamin adenosyltransferase. *Biochemistry. 45*, 15188–15196.
15. Saridakis, V., Yakunin, A., Xu, X., Anandakumar, P., Pennycooke, M., Gu, J., Cheung, F., Lew, J. M., Sanishvili, R., Joachimiak, A., Arrowsmith, C. H., Christendat, D., and Edwards, A. M. (2004) The structural basis for methylmalonic aciduria: The crystal structure of archeael ATP:cobalamin adenosyltransferase. *J. Biol. Chem. 279*, 23646–23653.
16. St Maurice, M., Mera, P., Park, K., Brunold, T. C., Escalante-Semerena, J. C., and Rayment, I. (2008) Structural characterization of a human-type corrinoid adenosyltransferase confirms that coenzyme B_{12} is synthesized through a four-coordinate intermediate. *Biochemistry. 47*, 5755–5766.
17. St Maurice, M., Mera, P. E., Taranto, M. P., Sesma, F., Escalante-Semerena, J. C., and Rayment, I. (2007) Structural characterization of the active site of the PduO-type ATP:co(I)rrinoid adenosyltransferase from *Lactobacillus reuteri*. *J. Biol. Chem. 282*, 2596–2605.
18. Mera, P. E., St Maurice, M., Rayment, I., and Escalante-Semerena, J. C. (2007) Structural and functional analyses of the human-type corrinoid adenosyltransferase (PduO) from *Lactobacillus reuteri*. *Biochemistry. 46*, 13829–13836.
19. Mera, P., St. Maurice, M., Rayment, I., and Escalante-Semerena, J. (2009) Residue Phe112 of the human-type corrinoid adenosyltransferase (PduO) enzyme of *Lactobacillus reuteri* is critical to the formation of the four-coordinate Co(II) corrinoid substrate and to the activity of the enzyme. *Biochemistry. 48*, 3138–3145.
20. Lexa, D., and Saveant, J.-M. (1983) The electrochemistry of vitamin B_{12}. *Acc. Chem. Res. 16*, 235–243.
21. Stich, T. A., Yamanishi, M., Banerjee, R., and Brunold, T. C. (2005) Spectroscopic evidence for the formation of a four-coordinate Co^{2+} cobalamin species upon binding to the human ATP:cobalamin adenosyltransferase. *J. Am. Chem. Soc. 127*, 7660–7661.
22. Mancia, F., Keep, N. H., Nakagawa, A., Leadlay, P. F., McSweeney, S., Rasmussen, B., Bösecke, P., Diat, O., and Evans, P. R. (1996) How coenzyme B_{12} radicals are generated: The crystal structure of methylmalonyl-coenzyme A mutase at 2 Å resolution. *Structure 4*, 339–350.
23. Hiratsuka, T. (1983) New ribose-modified fluorescent analogs of adenine and guanine nucleotides available as substrates for various enzymes. *Biochim. Biophys. Acta. 742*, 496–508.
24. Neal, S. E., Eccleston, J. F., and Webb, M. R. (1990) Hydrolysis of GTP by p21NRAS, the NRAS protooncogene product, is accompanied by a conformational change in the wild-type protein: Use of a single fluorescent probe at the catalytic site. *Proc. Natl. Acad. Sci. U.S.A. 87*, 3562–3565.
25. Fan, C., and Bobik, T. A. (2008) Functional characterization and mutation analysis of human ATP:cob(I)alamin adenosyltransferase. *Biochemistry. 47*, 2806–2813.
26. Padovani, D., and Banerjee, R. (2006) Protection and activation of the radical enzyme, methylmalonyl-CoA mutase by its chaperone. *Biochemistry. 45*, 9300–9306.
27. Padovani, D., Labunska, T., and Banerjee, R. (2006) Energetics of interaction between the G-protein chaperone, MeaB and B_{12}-dependent methylmalonyl-CoA mutase. *J. Biol. Chem. 281*, 17838–17844.
28. Korotkova, N., and Lidstrom, M. E. (2004) MeaB is a component of the methylmalonyl-CoA mutase complex required for protection of the enzyme from inactivation. *J. Biol. Chem. 279*, 13652–13658.
29. Nakamoto, R. K., Baylis Scanlon, J. A., and Al-Shawi, M. K. (2008) The rotary mechanism of the ATP synthase. *Arch. Biochem. Biophys. 476*, 43–50.